A migration velocity updating method based on the shot index common image gather and finite-frequency sensitivity kernel

Xiao-Bi Xie and Hui Yang, Institute of Geophysics and Planetary Physics, University of California, Santa Cruz, CA 95064, USA.*

Summary

We introduce a new tomography method for migration velocity updating. The method is based on the sensitivity analysis of finite-frequency signals. We derive the finite-frequency sensitivity kernels particularly for the migration residual moveout in shot-domain common image gathers. We validate these sensitivity kernels by comparing them with the residual moveout directly measured from the migrated image. Based on these sensitivity kernels, we build an inversion system for velocity updating. Using synthetic data sets, we successfully invert velocity perturbations from the residual moveout in shot-domain common image gathers.

Introduction

A seismic survey conducted in the real world generates data for subsurface imaging. Due to the lack of an accurate model, the image is usually incoherent. The distortion of the image contains important information about errors in the migration velocity model. The migration velocity updating links the coherence in the image to errors in the model and modifies the model towards the true model. Mean time, this process improves the quality of the image.

The information for migration velocity analysis is the migration residual moveout (RMO) in different common image gathers (CIGs) (e.g., shot-domain, offset-domain or angle-domain CIGs). Different methods have been developed for extracting information from the RMO in CIGs, and to convert this information into model corrections. The parameterized RMO measurement methods (Mosher, et al., 2001; Jiao, et al., 2002) are stable and robust. However, they usually adopt simple model geometries and lack the capability to deal with models with strong lateral variations. Other more sophisticated techniques use tomography inversion to update the velocity model (Bishop, 1985; Brandsberg-Dahl, et al., 2003). Based on the ray-tracing technique, the RMO information is converted to the velocity correction through back projection along the rays. However, these methods have serious drawbacks in complex depth imaging problems due to their high-frequency asymptotic feature (Biondi, 2006). To build a migration velocity updating algorithm under the full wave theory and include all dynamic and kinematic information in the image for inversion is very attractive (Biondi and Symes, 2004; Sava and Biondi, 2004). However, such jobs are not easy and many of them are still under development.

Recently, the sensitivity of finite-frequency signals to velocities has been investigated by researchers working in both earthquake seismology (Dahlen et al., 2000; Huang, et al., 2000; Zhao, et al., 2000) and applied seismology (Woodward, 1992; Spetzler and Snieder, 2004; Sava and Biondi, 2004; Jocker, et al., 2006). Finite-frequency sensitivity kernels have been used for solving many tomography problems. In this paper, based on the finite-frequency sensitivity theory, we develop a new migration velocity updating method which considers the wave phenomena while still keeping the simplicity of ray-based methods. We first derive the sensitivity kernel for shot-domain RMO. Based on this sensitivity kernel, an inversion system is built to calculate velocity correction from the observed RMO. Synthetic data sets are used to validate this sensitivity kernel and velocity model inversion.

The Sensitivity Kernel for Shot-Domain RMO

Assume that there is a true velocity model $v_T(\mathbf{r})$ which can be expressed as $v_T(\mathbf{r}) = v_0(\mathbf{r}) + \delta v(\mathbf{r})$,where $v_0(\mathbf{r})$ is a starting model reasonably closing to $v_T(\mathbf{r})$, and $\delta v(\mathbf{r})$ is the difference between the starting and the true velocity models. The seismic survey is conducted in the true velocity model. It uses a source located at $\mathbf{r}_S$ to generate a down going wave $u_D^T(\mathbf{r};\mathbf{r}_S)$. After interacting with subsurface targets, the down going wave generates a reflection wave $u_U^T(\mathbf{r};\mathbf{r}_S)$ carrying the information of structures. In practice, both the true velocity and the target location are unavailable. We conduct migration in the starting model $v_0(\mathbf{r})$ and obtain an image

$$I(\mathbf{r}_I,\mathbf{r}_S) = u_D^0(\mathbf{r}_I;\mathbf{r}_S)\,u_U^0(\mathbf{r}_I;\mathbf{r}_S)^* \qquad (1)$$

where $u_D^0(\mathbf{r};\mathbf{r}_S)$ and $u_U^0(\mathbf{r};\mathbf{r}_S)$ are down and up going waves calculated in the starting model, the asterisk denotes the complex conjugate, $u_U^0(\mathbf{r}_I;\mathbf{r}_S)^*$ is the frequency domain equivalent of time reversed original reflection wave, $\mathbf{r}_I$ is the image point which is usually shifted from the true target location. At $\mathbf{r}_I$, the phase error between the image generated using the starting model and true velocity model is

$$\delta\varphi(\mathbf{r}_I,\mathbf{r}_S) = \arg\left\{\frac{u_D^T(\mathbf{r}_I;\mathbf{r}_S)}{u_D^0(\mathbf{r}_I;\mathbf{r}_S)}\right\} + \arg\left\{\frac{u_U^T(\mathbf{r}_I;\mathbf{r}_S)^*}{u_U^0(\mathbf{r}_I;\mathbf{r}_S)^*}\right\} \qquad (2)$$

where $\delta\varphi$ is the phase error caused by the inaccurate velocity model. Using Rytov approximation (e.g., Jocker et al., 2006), we have

$$\delta\varphi(\mathbf{r}_I,\mathbf{r}_S)=\text{imag}\left\{\frac{U_D(\mathbf{r}_I;\mathbf{r}_S)}{u_D^0(\mathbf{r}_I;\mathbf{r}_S)}+\frac{U_U(\mathbf{r}_I;\mathbf{r}_S)^*}{u_U^0(\mathbf{r}_I;\mathbf{r}_S)^*}\right\}, \quad (3)$$

where $U_D(\mathbf{r}_I,\mathbf{r}_S)$ and $U_U(\mathbf{r}_I,\mathbf{r}_S)$ are scattering waves caused by the velocity difference $\delta v(\mathbf{r})$.

The purpose of migration velocity updating is estimating the velocity error $\delta v(\mathbf{r})$ based on observed $\delta\varphi$ or its equivalents. In order to do this, we creat a relationship between these two parameters. Using the scattering theory,

$$U_D(\mathbf{r}_I,\mathbf{r}_S)=2k_0^2S\int_V m(\mathbf{r}')G_D(\mathbf{r}';\mathbf{r}_S)G(\mathbf{r}';\mathbf{r}_I)dv', \quad (4)$$

$$U_U(\mathbf{r}_I,\mathbf{r}_S)^*=2k_0^2S\int_V m(\mathbf{r}')G_U^*(\mathbf{r}';\mathbf{r}_S)G(\mathbf{r}';\mathbf{r}_I)dv', \quad (5)$$

where $m(\mathbf{r})=\delta v/v_0(\mathbf{r})$, $k_0=\omega/v_0(\mathbf{r})$ and S is the source spectrum, G is the Green's function, G_D and G_U are Green's functions for source wave and reflections, all are calculated in the starting model. The spatial integral $\int_V dv'$ includes all regions with velocity perturbations. Substituting equations (4)-(5) into equation (3), we have $\delta\varphi=\delta\varphi_D+\delta\varphi_U$, and

$$\delta\varphi_D(\mathbf{r}_I,\mathbf{r}_S)=\int_V m(\mathbf{r}')K_D^F(\mathbf{r}',\mathbf{r}_S,\mathbf{r}_I)dv', \quad (6)$$

$$\delta\varphi_U(\mathbf{r}_I,\mathbf{r}_S)=\int_V m(\mathbf{r}')K_U^F(\mathbf{r}',\mathbf{r}_S,\mathbf{r}_I)dv', \quad (7)$$

where integrands

$$K_D^F(\mathbf{r},\mathbf{r}_S,\mathbf{r}_I)=\text{imag}\left[2k_0^2\frac{G_D(\mathbf{r};\mathbf{r}_S)G(\mathbf{r};\mathbf{r}_I)}{G_D(\mathbf{r}_I;\mathbf{r}_S)}\right], \quad (8)$$

$$K_U^F(\mathbf{r},\mathbf{r}_S,\mathbf{r}_I)=\text{imag}\left[2k_0^2\frac{G_U^*(\mathbf{r};\mathbf{r}_S)G(\mathbf{r};\mathbf{r}_I)}{G_U^*(\mathbf{r}_I;\mathbf{r}_S)}\right] \quad (9)$$

are frequency domain sensitivity or Fréchet kernels for both source and receiver sides. Equations (6)-(9) give the relationship between the velocity perturbations and the phase errors in the migration image.

In time or depth domains, the observations are usually broadband delay time or moveout. In this case, the delay time can be obtained as

$$\delta t_D(\mathbf{r}_I,\mathbf{r}_S)=\int_V m(\mathbf{r}')K_D^B(\mathbf{r}',\mathbf{r}_S,\mathbf{r}_I)dv', \quad (10)$$

$$\delta t_U(\mathbf{r}_I,\mathbf{r}_S)=\int_V m(\mathbf{r}')K_U^B(\mathbf{r}',\mathbf{r}_S,\mathbf{r}_I)dv', \quad (11)$$

where

$$K_D^B(\mathbf{r},\mathbf{r}_S,\mathbf{r}_I)=\int\frac{A(\omega)}{\omega}K_D^F(\mathbf{r},\mathbf{r}_S,\mathbf{r}_I,\omega)d\omega, \quad (12)$$

$$K_U^B(\mathbf{r},\mathbf{r}_S,\mathbf{r}_I)=\int\frac{A(\omega)}{\omega}K_U^F(\mathbf{r},\mathbf{r}_S,\mathbf{r}_I,\omega)d\omega \quad (13)$$

are broadband delay-time sensitivity kernels of the source and receiver sides. $A(\omega)$ is a frequency dependent weighting function with its actual form dependent on how the delay time or moveout is measured. For example, the source power spectrum can be used if the delay time is measured using the cross correlation.

Under the small perturbation, the RMO can be related to the travel time delay via

$$R(\mathbf{r}_I,\mathbf{r}_S)=-\frac{v_0(\mathbf{r}_I)}{2\cos[\theta(\mathbf{r}_I,\mathbf{r}_S)]}\delta t(\mathbf{r}_I,\mathbf{r}_S), \quad (14)$$

where $R(\mathbf{r}_I,\mathbf{r}_S)$ is the observed RMO along the reflector normal, $\theta(\mathbf{r}_I,\mathbf{r}_S)$ is the reflection angle relative to the reflector normal, $v_0(\mathbf{r}_I)$ is the local velocity at $\mathbf{r}_I$, and $\delta t(\mathbf{r}_I,\mathbf{r}_S)$ is the corresponding travel time delay. Equations (8)-(14) link the observed RMO to the velocity difference.

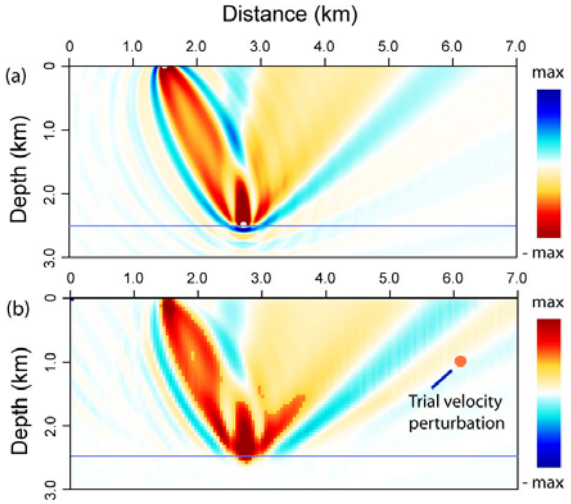

Figure 1. A sensitivity kernel for a shot gather image, with (a) theoretical sensitivity kernel, and (b) the sensitivity map directly measured from migration imaging.

Inversion System

To build an inversion system, we partition the model and sensitivity kernels to generate a linear system

$$R(\mathbf{r}_I,\mathbf{r}_S)=-\frac{v_0(\mathbf{r}_I)}{2\cos[\theta(\mathbf{r}_I,\mathbf{r}_S)]}\times\sum_i m(\mathbf{r}_i)\left[K_D^B(\mathbf{r}_i,\mathbf{r}_S,\mathbf{r}_I)+K_U^B(\mathbf{r}_i,\mathbf{r}_S,\mathbf{r}_I)\right], \quad (15)$$

where

$$K_D^B(\mathbf{r}_i,\mathbf{r}_S,\mathbf{r}_I)=\int_{V(\mathbf{r}_i)}K_D^B(\mathbf{r}',\mathbf{r}_S,\mathbf{r}_I)dv' \quad (16)$$

$$K_U^B(\mathbf{r}_i,\mathbf{r}_S,\mathbf{r}_I)=\int_{V(\mathbf{r}_i)}K_U^B(\mathbf{r}',\mathbf{r}_S,\mathbf{r}_I)dv' \quad (17)$$

are discretized kernels, $V(\mathbf{r}_i)$ is a subspace of V and is indexed by its location $\mathbf{r}_i$, $m(\mathbf{r}_i)$ is the unknown velocity perturbation at the partitioned subspace. In practice, the absolute RMOs are often unavailable. Instead, the data we directly observed are relative RMOs between different shots

$$\delta R(\mathbf{r}_{S1},\mathbf{r}_{S2},\mathbf{r}_I) = R(\mathbf{r}_{S2},\mathbf{r}_I) - R(\mathbf{r}_{S1},\mathbf{r}_I), \quad (18)$$

where $\delta R(\mathbf{r}_{S1},\mathbf{r}_{S2},\mathbf{r}_I)$ is the relative RMO, and $\mathbf{r}_{S1}$ and $\mathbf{r}_{S2}$ are two different shot indexes in the same CIG. For relative RMO data, the linear system (15) becomes

$$\delta R(\mathbf{r}_{S1},\mathbf{r}_{S2},\mathbf{r}_I) = -\sum_i m(\mathbf{r}_i) K^B(\mathbf{r}_i,\mathbf{r}_{S1},\mathbf{r}_{S2},\mathbf{r}_I), \quad (19)$$

where

$$K^B(\mathbf{r}_i,\mathbf{r}_{S1},\mathbf{r}_{S2},\mathbf{r}_I) = \frac{v_0(\mathbf{r}_I)}{2\cos\left[\theta(\mathbf{r}_{S2},\mathbf{r}_I)\right]}\left[K_D^B(\mathbf{r}_i,\mathbf{r}_{S2},\mathbf{r}_I) + K_U^B(\mathbf{r}_i,\mathbf{r}_{S2},\mathbf{r}_I)\right] \quad (20)$$

$$-\frac{v_0(\mathbf{r}_I)}{2\cos\left[\theta(\mathbf{r}_{S1},\mathbf{r}_I)\right]}\left[K_D^B(\mathbf{r}_i,\mathbf{r}_{S1},\mathbf{r}_I) + K_U^B(\mathbf{r}_i,\mathbf{r}_{S1},\mathbf{r}_I)\right]$$

is the broadband differential kernel. In equation (19), $(\mathbf{r}_{S1},\mathbf{r}_{S2},\mathbf{r}_I)$ is the index for RMO data and $(\mathbf{r}_i)$ is the index for unknown velocity perturbations. Once we have the relative RMO data $\delta R(\mathbf{r}_{S1},\mathbf{r}_{S2},\mathbf{r}_I)$ and the differential kernel $K^B(\mathbf{r}_i,\mathbf{r}_{S1},\mathbf{r}_{S2},\mathbf{r}_I)$ calculated from starting model $v_0(\mathbf{r})$, we can invert the velocity perturbation $m(\mathbf{r}_i)$ and use it to update the starting model.

Numerical Examples

Sensitivity Analysis. To check the theory, we calculate the sensitivity kernel for a simple scenario and compare it with the result from direct moveout measurements. Shown in Figure 1a are broadband delay-time sensitivity kernels calculated using equations (12)-(13) for a 10 Hz Ricker wavelet and a pair of shot and image locations in a constant velocity model. To validate this sensitivity kernel, we generate a shot gather synthetic data set for this model; conduct migration and measure the RMO at the image point. To introduce an error in the migration velocity model, we add a small round trial velocity perturbation in the original constant velocity model. The trial perturbation (shown as a small solid circle in 1b) has a diameter of 200 m and a velocity perturbation of 20%. We move this trial perturbation around the entire model. At each location, a migration is conducted and the RMO is measured. We then use these RMO records to generate a sensitivity map shown in Figure 1b. Note that the positive delay time causes a negative moveout given the downward moveout as positive. The theoretical kernel is satisfactorily consistent with the direct measured sensitivity. The source side sensitivity kernel is similar to the conventional Fréchet kernel for a pair of point source and point receiver. However, the receiver side kernel is quite different. It has a large opening towards the up direction. Near the source location and immediately above the image point, there are two sensitive regions where the velocities strongly affect the delay time. Regions along the center of these kernels, where the traditional ray path is, show relatively weak sensitivity. There are positive sensitivities around the main lobes of the kernels, indicating the positive velocity perturbation in these regions causes positive time delay. The result shows quite complex sensitivity of the RMO to the velocity. The regions within which the velocity can affect the RMO is much broader than that predicted by the high-frequency ray, indicating the conventional ray-based methods may encounter difficulty in velocity updating.

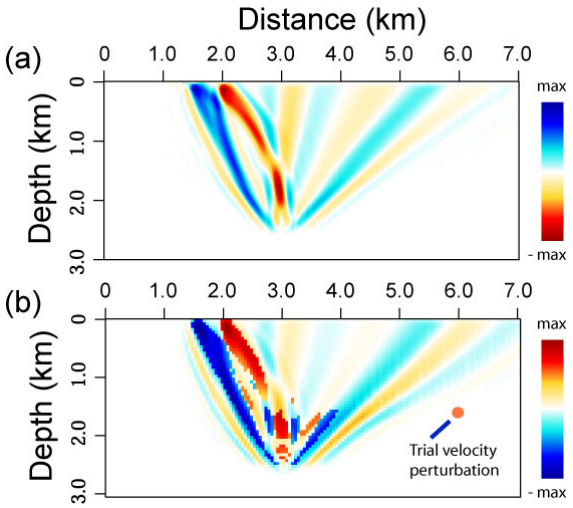

Figure 2. A broadband differential sensitivity kernel for a variable background velocity model, with (a) the theoretical kernel, and (b) directly measured sensitivity map for RMO.

Shown in Figure 2a is a 17.5 Hz broadband differential sensitivity kernel for two sources in a model with about 30% velocity changes. The kernel is calculated using equation (20) and the one-way and one-return approximation (Xie and Wu, 2001; Wu, et al., 2006). Note its complex features resulted from a positive and a negative shot kernel. Shown in 2b is the sensitivity map measured from the migration image. The consistency between these maps further confirms the validity of these kernels.

Inversion in a constant background velocity. Shown in Figure 3 is the inversion result for a constant background velocity model. The true velocity model in 3a is composed of a 3.5 km/s background velocity and 4 Gaussian shaped velocity perturbations located at the middle of the model. The maximum velocity perturbations are +10% at the centers of these patches. The synthetic data set is generated

using the true velocity model and a 17.5 Hz Ricker wavelet. The migration is calculated using the background model and resulted RMO data are used in the inversion. Shown in 3b are locations of the 9 shots and 17 image points used in generating data, as well as the perturbations descretized using 0.3 km x 0.3 km grid. We target our inversion within a 1.5 km x 1.5 km region and left the rest of the model unperturbed. A similar partition is used in the inversion and the result is shown in 3c. Comparing Figure 3c with 3b, the inverted velocity perturbation reproduces the main features of the model, even for the smallest patch.

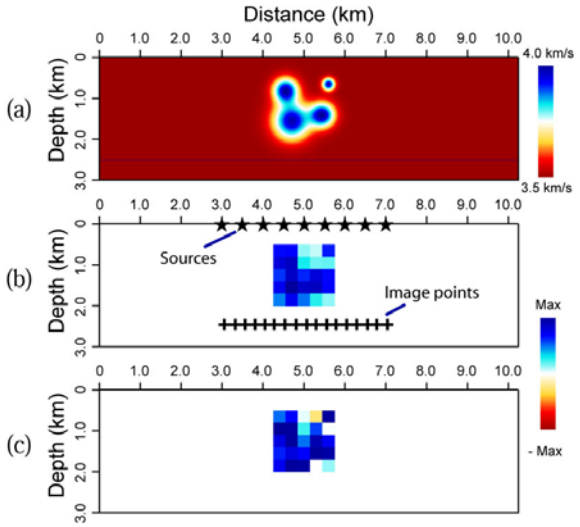

Figure 3. Inversion for constant background velocity model, with (a) true velocity model, (b) descretized velocity perturbation, and (c) inverted perturbations.

Inversion in a variable background velocity. Shown in Figure 4 is the inversion result for a variable background velocity model. The true velocity model in 4a is composed of the background velocity in 4b and the checkerboard shaped velocity perturbations in 4c. The background velocity varies between 3.0 and 4.1 km/s, and the perturbation has maximum ±5% velocity variations overlapped on the background velocity. The synthetic data set is generated using the true velocity. The migration is calculated using the background model and the RMO data is used in the inversion. A total of 8 shots and 8 image points shown in 4c are used in the inversion. We limit our inversion within the dashed rectangle shown in 4c. Figure 4d is the inverted velocity perturbation which has the correct pattern of the original perturbations.

Discussion and Conclusions

A special finite-frequency sensitivity kernel is derived for the RMO of shot-domain CIG. Based on this, we build an inversion system which links the observed RMO to the velocity model errors. Synthetic data sets are used to validate the sensitivity kernels and to test the inversion system. Inversions are conducted in both constant and variable background velocity models. The results show that the finite-frequency kernels correctly predict the velocity sensitivity of the depth image, and the inversion has very good resolution on small scale velocity perturbations. The new method is wave equation based and is naturally formulated for the shot-domain CIG. No expensive angle domain analysis or ray tracings are required.

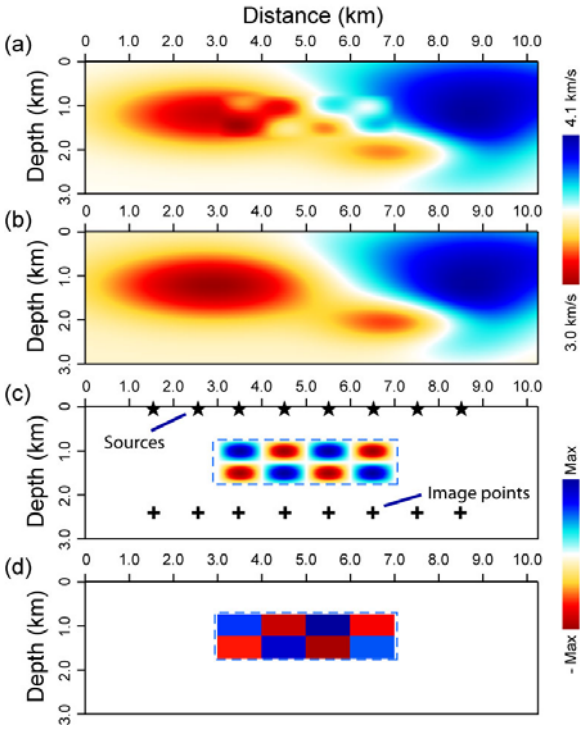

Figure 4. Inversion for variable background model, with (a) true velocity model, (b) background velocity model, (c) velocity perturbation, and (d) inverted perturbation.

All calculations at this moment are conducted close to the linear condition. For a more general circumstance, where the starting model is strongly biased from the true velocity model, linearization and multi-step iterations are required. The numerical examples are for 2D models. However, there is no major obstacle to generalize these calculations to a 3D problem.

Acknowledgement

This research is supported by the DOE/BES project at the University of California, Santa Cruz under the Grant No. DE-FG02-04ER15530. The facility support from the W.M. Keck Foundation is also acknowledged.

EDITED REFERENCES

Note: This reference list is a copy-edited version of the reference list submitted by the author. Reference lists for the 2007 SEG Technical Program Expanded Abstracts have been copy edited so that references provided with the online metadata for each paper will achieve a high degree of linking to cited sources that appear on the Web.

REFERENCES

Biondi, B., 2006, 3D seismic imaging: SEG.

Biondi, B., and W. W. Symes, 2004, Angle-domain common-image gathers for migration velocity analysis by wavefield-continuation imaging: Geophysics, 69, 1283–1298

Bishop, T. N., K. P. Bube, R. T. Cutler, R. T. Langan, P. L. Love, J. R. Resnick, R. T. Shuey, D. A. Spindler, and H. W. Wyld, 1985, Tomographic determination of velocity and depth in laterally varying media: Geophysics, 50 , 903–923.

Brandsberg-Dahl, S., B. Ursin, and M. V. De Hoop, 2003, Seismic velocity analysis in the scattering angle/azimuth domain: Geophysical Prospecting, 51 , 295–314.

Dahlen, F., S. Huang, and G. Nolet, 2000, Frechet kernels for finite-frequency travel times – I, theory: Geophysical Journal International, 141, 157–174.

Huang, S., F. Dahlen, and G. Nolet, 2000, Frechet kernels for finite-frequency travel times – II, examples: Geophysical Journal International, 141, 175–203.

Jiao, J., P. L. Stoffa, M. K. Sen, and R. K. Seifoullaev, 2002, Residual migration-velocity analysis in the plane-wave domain: Geophysics, 67, 1252–1269.

Jocker, J., J. Spetzler, D. Smeulders, and J. Trampert, 2006, Validation of first-order diffraction theory for the traveltimes and amplitudes of propagating waves: Geophysics, 71, no. 6, T167–T177.

Mosher, C., S. Jin, and D. Foster, 2001, Migration velocity analysis using common angle image gathers: 71st Annual International Meeting, SEG, Expanded Abstracts, 889–892.

Sava, P. C., and B. Biondi, 2004, Wave-equation migration velocity analysis - I: theory: Geophysical Prospecting, 52, 593–606.

Spetzler, J., and R. Snieder, 2004, The Fresnel volume and transmitted waves: Geophysics, 69, 653–663.

Woodward, M. J., 1992, Wave-equation tomography: Geophysics, 57, 15–26.

Wu, R. S., X. B. Xie, and X. Y. Wu, 2006, One-way and one-return approximations (de Wolf approximation) for fast elastic wave modeling in complex media, in R. S. Wu and V. Maupin, eds., Advances in Wave Propagation in Heterogeneous Earth: Elsevier, 265–322.

Xie, X. B., and R. S. Wu, 2001, Modeling elastic wave forward propagation and reflection using the complex screen method: Journal of the Acoustical Society of America, 109, 2629–2635.

Zhao, L., T. H. Jordan, and C. H. Chapman, 2000, Three-dimensional Frechet differential kernels for seismic delay times: Geophysical Journal International, 141, 558–576.